J Mater Sci (2010) 45:1242–1247
DOI 10.1007/s10853-009-4073-8

Structural and electrical conductivity studies on undoped and copper-doped nanocrystalline zinc sulphide

S. Chellammal · S. Sankar · S. Selvakumar · E. Viswanathan · R. Murugaraj · K. Sivaji

Received: 1 July 2009 / Accepted: 22 November 2009 / Published online: 11 December 2009

Abstract Zinc sulphide (ZnS) and copper-doped zinc sulphide nanocrystallites (ZnS:Cu) of average size 4 and 3 nm, respectively, have been synthesized by chemical precipitation method. Structural and morphological studies using X-ray and high resolution transmission electron microscopy (HRTEM) measurements have confirmed hexagonal structure for the samples. Using impedance spectroscopy, the effect of grain interior and grain boundary regions on the electrical conductivity have been studied at various temperatures. In the high temperature region, the grain boundary contribution to conduction is found to be larger than that of the grain interior region. Further, the activation energies of charge carriers in both the grain interior and grain boundary regions have been determined. The conduction mechanism of copper-doped zinc sulphide nanocrystallites have been studied at various temperatures and the results are reported.

Introduction

A systematic study of size effect on the impedance properties of semiconducting nanocrystallites is essential for proper understanding of their technological applications [1–3]. Nanocrystalline metal chalcogenides exhibit very interesting electronic structure and transition probabilities [4–6] and also many applications in the field of spintronics [7]. Among the II–VI semiconductors, zinc sulphide is widely studied owing to its stability and technological applications [8, 9]. Zinc sulphide nanoparticles doped with metallic elements has a variety of applications [10]. Several studies on the interesting optical properties of metal-doped ZnS nanoparticles have been reported in recent years [11–14]. On the other hand, studies on the characterization of electrical properties of metal-doped ZnS nanoparticles are seldom found. Present studies are, hence, devoted towards the impedance analysis of undoped and copper-doped ZnS nanoparticles.

Zinc sulphide is a direct band gap semiconductor with a band gap of $\sim$3.7 eV [14]. Powder samples of undoped and copper-doped ZnS (ZnS:Cu) nanocrystallites have been prepared in the present work by chemical precipitation method. X-ray characterization of the prepared nanocrystallites has been carried out for the confirmation of structure and also to obtain the average size of the nanocrystallites and these results are compared with the high resolution transmission electron microscopic (HRTEM) studies. The doping concentration of copper in ZnS has been estimated by energy dispersive X-ray analysis (EDAX). Impedance measurements have been carried out in order to characterize the electrical properties of the sample over a temperature range from 573 to 873 K and the results are discussed and reported in the present paper.

Experimental

Sample preparation

Chemical precipitation of copper-doped ZnS nanocrystallites has been carried out at room temperature, using the

S. Chellammal · S. Sankar (✉)
Department of Physics, College of Engineering, Anna University, Guindy, Chennai 600 025, Tamil Nadu, India
e-mail: ssankar@annauniv.edu

S. Selvakumar · E. Viswanathan · K. Sivaji
Department of Nuclear Physics, University of Madras, Guindy Campus, Chennai 600 025, Tamil Nadu, India

R. Murugaraj
Department of Physics, Madras Institute of Technology Campus, Anna University, Chennai 600 044 Tamil Nadu, India

reactants anhydrous zinc chloride ($ZnCl_2$) and anhydrous sodium sulphide (Na_2S) with ethylene glycol as capping agent. Doping of copper has been done by adding copper chloride solution (0.005 M) with zinc chloride solution. The preparation was carried out over a reflux time of 600 s for 100 mL volume of the reacting solutions. The precipitate was then centrifuged and washed with de-ionized water repeatedly, and then with methanol, finally. Then the precipitate was dried under vacuum.

Structural characterization

Powder X-ray diffraction studies were carried out using Mo Kα radiation ($\lambda = 0.070930$ nm) (Philips 2275/20 X-ray diffractometer) to determine the structural phase of the sample. High resolution transmission electron microscopic (model: JEOL 3010 operated at 300 kV with a resolution of 0.14 nm) measurements were carried out to obtain the morphological characteristics of the sample. Energy dispersive X-ray analysis (EDAX) (Leo stereo scan 440 model) has been used to estimate the percentage of the dopant (Cu) content in ZnS:Cu nanocrystallites.

Electrical characterization

Complex impedance $|(Z,\theta)|$ measurements have been carried out in a sample pellet of $\sim$8 mm diameter and $\sim$1.5 mm thickness as a function of frequency (from 1 Hz to 1 MHz) at different temperatures (from 573 to 873 K), by using an Impedance/Grain-Phase Analyzer (SOLARTRON 1260) with platinum electrodes.

The impedance analyzer was connected to a dedicated computer with software to acquire the impedance data. The whole setup of sample compartment inside the furnace was evacuated to 1×10^{-5} Torr, in order to prevent oxidation of sample during heating. Heating rate was maintained at 2 K/min. The temperature of the furnace was measured with a resolution of ±1 K using a Eurotherm (818 P) PID temperature controller. The data collected during both heating and cooling cycles have been found to be highly consistent.

The conductivity (σ), the real (ε'), and imaginary (ε'') parts of the dielectric constant (ε^*) as well as real (M') and imaginary (M'') parts of the complex modulus (M^*) were obtained from the relations,

$$\epsilon^*(\omega) = \epsilon'(\omega) - i\epsilon''(\omega) = 1/i\omega C_0 Z^*(\omega),$$

$$\sigma^*(\omega) = \sigma'(\omega) + i\sigma''(\omega) = i\omega\epsilon_0\epsilon^*(\omega),$$

and

$$M^*(\omega) = M'(\omega) + iM''(\omega) = 1/\epsilon^*(\omega).$$

where ω is the angular frequency, C_0 ($C_0 = \varepsilon_0 A/d$) is the vacuum capacitance, ε_0 is the free space dielectric permittivity, A is the cross-sectional area of the sample, and d is the thickness of the sample.

Results and discussion

The powder XRD patterns of the synthesized nanocrystalline ZnS and ZnS:Cu samples are presented in Fig. 1a and b. The four peaks observed at 2θ values equal to 12.225, 20.625, 24.525, and 33.925 for ZnS sample and 12.216, 20.646, 24.531, and 33.914 for ZnS:Cu sample have been identified to be due to the planes with the indices (1 0 0), (1 1 0), (2 0 0), and (2 1 1), respectively, of the hexagonal structural phase of ZnS (JCPDS PDF No:011280) [15]. Reduction of particle size leads to the broadening of line widths and weakening in the line intensities of reflection from high index (211) planes which is comparable to that of the noise reflections. Similar results were reported by Mazher et.al. for ZnSe nanoparticles [16]. However, the intensity level of the noise peaks is much smaller than the 100% peak ((1 0 0) planes) as shown in Fig. 1a and b.

The present samples have been prepared at room temperature (27 °C) while those of the earlier studies [8, 9] involved considerable heating of the reactants during preparation. The average grain size of the samples has been calculated from the powder XRD data using the Scherrer formula [17] as 4 nm for ZnS and as 3 nm for ZnS:Cu sample. Copper-doped ZnS (i.e., ZnS:Cu) has its average

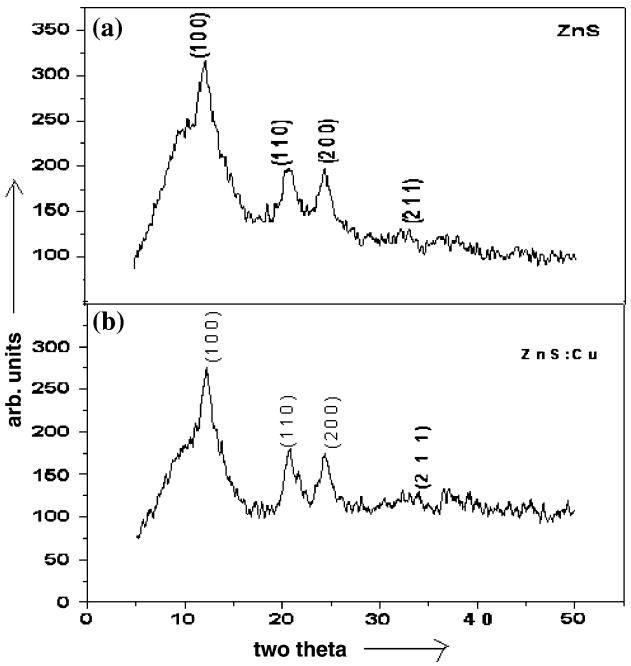

Fig. 1 Powder X-ray diffractograms of the as-prepared nanocrystalline **a** ZnS and **b** ZnS:Cu

size reduced considerably when compared to that of ZnS and is in good agreement with the result of Wang et al. [18] that copper doping has the effect of reducing the average particle size in ZnS.

The HRTEM microstructures, lattice fringe patterns, and electron diffraction rings of the nanocrystalline ZnS are displayed in Fig. 2a–c and those of ZnS:Cu samples are presented in Fig. 3a–c, respectively. The HRTEM microstructures in Figs. 2a and 3a show the homogeneity of size distribution in the samples; however, the ZnS:Cu particles are found to be agglomerated which may be due to the presence of copper. In both the cases, the observed nanoparticles are nearly spherical. Their crystalline nature is evident from their lattice fringe patterns (Figs. 2b and 3b). The lattice planes yielding the rings of the selected area electron diffraction are indexed to (1 0 0), (1 1 0), (2 0 0), and (2 1 1) planes of the hexagonal phase of the samples. These results hence are in agreement with the X-ray diffraction studies.

The average size of the ZnS and ZnS:Cu nanocrystallites and their *d*-spacing values obtained by powder XRD studies for the samples are also compared with the corresponding sizes obtained from HRTEM measurements. It is worth pointing out here that Borchert et al. [19] have demonstrated clearly that the average size of nanocrystallites can more reliably be obtained from XRD studies by Scherrer formula than the other size-measuring techniques such as HRTEM and small angle X-ray scattering (SAXS) studies. Hence, in accordance with Borchert et al. [19], we have estimated the average size (d) of our present nanocrystalline samples using the Scherrer formula.

$$d = 0.9K\lambda/\omega\mathrm{Cos}\theta \quad (1)$$

where the factor $K = 4/3$ accounts for the quasi-spherical geometry of the nanocrystallites, λ is the wavelength of X-rays used, ω is the width on 2θ scale, and θ is the scattering angle of X-rays. The above formula was also used by Nanda et al. [10] earlier to estimate the size of semiconductor nanocrystals reliably. Hence, we have also estimated the size of ZnS and ZnS:Cu nanocrystals in the present work using the above formula (Eq. 1). The results indicate that ZnS:Cu nanocrystallites have slightly decreased crystallite size and it is attributed to the doping of copper (Cu), since the conditions of sample preparation are identical for both the ZnS and ZnS:Cu samples. Due to change of volume fraction, the size of a particle has decreased by the relation

$$\text{Volume fraction } = 1 - (1 - 1/d)^2 \quad (2)$$

where d is the average crystallite size of the sample. This observation agrees well with that of Wang et al. [18] as mentioned earlier. The *d*-spacing values obtained from the powder XRD studies are presented in Table 1 for ZnS and ZnS:Cu samples and are also compared with the corresponding sizes obtained from HRTEM studies.

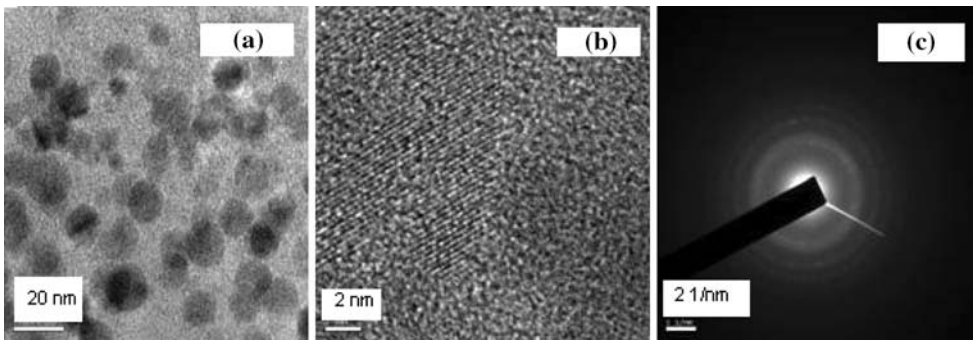

Fig. 2 **a** HRTEM microstructure, **b** lattice fringe pattern, and **c** electron diffraction rings of nanocrystalline ZnS

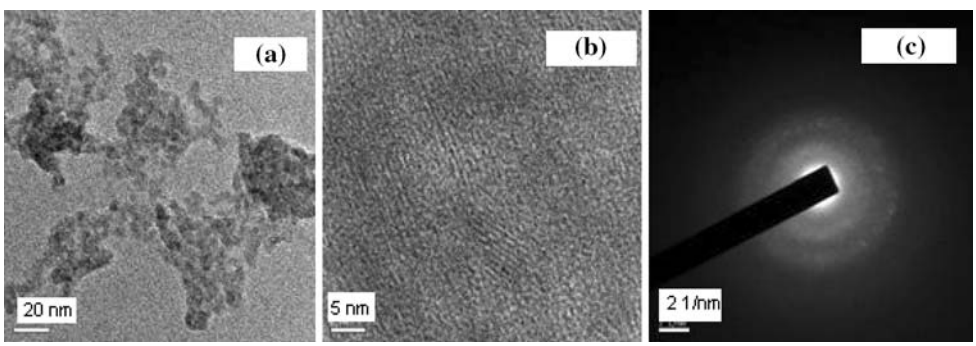

Fig. 3 **a** HRTEM microstructure, **b** lattice fringe pattern, and **c** electron diffraction rings of nanocrystalline ZnS:Cu

Table 1 Experimental and theoretical inter-planer spacing (d values)

(h k l) planes	d Spacing			Parameters (Å)
	XRD (Å)	HRTEM (Å)	Theoretically (Å)	
1 0 0	3.31	3.28	3.30	$a = 3.811$
1 1 0	1.92	1.90	1.90	$c = 6.234$
2 0 0	1.66	1.67	1.65	
2 1 1	1.22	1.23	1.22	

Table 1 shows results of the calculation of d-spacing by powder XRD, HRTEM, and using equation

$$d_{\mathrm{hkl}} = 1/\left(\left(h^2 + k^2 + hk\right)4/3a^2 + l^2/c^2\right)^{1/2} \quad (3)$$

theoretically for the prepared samples. The results of Table 1 confirm the hexagonal structure of the samples.

Energy dispersive X-ray analysis studies for the as-prepared ZnS and ZnS:Cu samples are presented in Fig. 4a and b, respectively. The percentage of the dopant (Cu) present has been found to be 0.20% in ZnS:Cu sample. Further, Table 2 gives the percentage of elements present in the ZnS and ZnS:Cu samples as obtained from the EDAX studies.

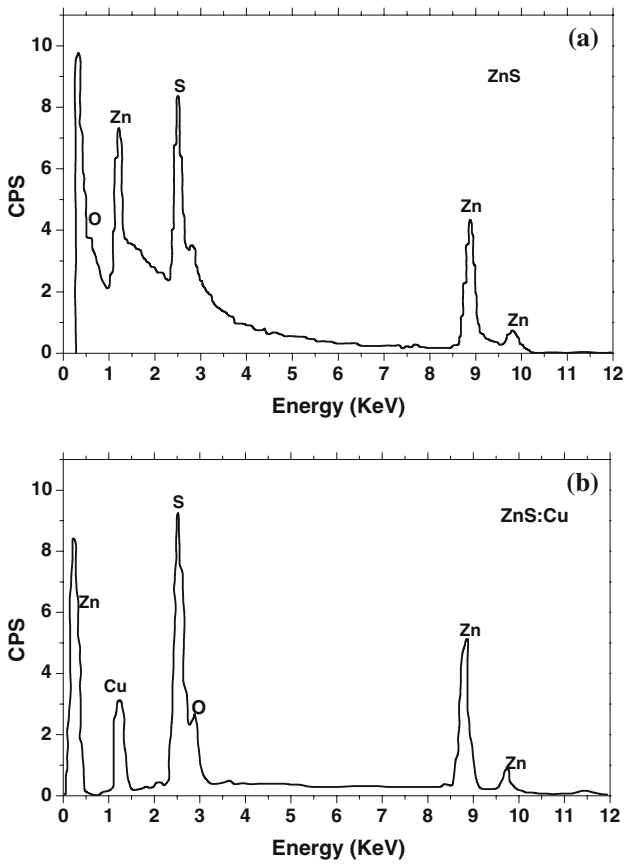

Fig. 4 EDAX pattern for **a** ZnS and **b** ZnS:Cu samples

Table 2 Percentage of elements present in ZnS and ZnS:Cu samples obtained from EDAX studies

Elements	Spectrum type	Elements (%)	Atomic (%)
For ZnS nanocrystallites			
O	ED	10.62	10.41
S	ED	39.88	40.67
Zn	ED	49.50	48.92
For ZnS–Cu-doped nanocrystallites			
S	ED	19.20	32.62
Cu	ED	1.86	1.60
Zn	ED	78.94	65.79

In general, the three characteristic semicircular arcs of the impedance spectra represent the results for high, intermediate, and low frequency regions. These are correlated to grain interior region, grain boundary region of the sample, and electrode-sample interface effects, respectively [20–23]. Figure 5a–c shows the impedance spectra for various temperature regions of ZnS sample. Figure 6a–c shows the impedance spectra for various temperature regions of prepared ZnS:Cu sample.

At low temperature region, that is 300 to 350 °C, the resistance varies from 8.57×10^6 to 3.65×10^5 ohm and the relaxation time changes from 1.28×10^{-3} to 1.56×10^{-5} s for ZnS: Cu sample. In this temperature region, single semicircular arcs only are observed for both ZnS and ZnS:Cu samples as in Figs. 5a and 6a, respectively. Hence the relaxation times of grain and grain boundary regions are almost equal for both the samples. In this region, a low conductivity is observed in the samples.

As the temperature is further increased from 400 to 420 °C, the resistance value of grain is found to be 1.23×10^5 ohm and that of the grain boundary is 2.63×10^5 ohm and the corresponding relaxation times are 1.53×10^{-6} and 2.39×10^{-6} s for ZnS:Cu sample. Figures 5b and 6b show, for both the samples, the presence of two well-resolved semicircular arcs and it implies that there exist two distinct relaxation processes, one for the grain interior region and the other for the grain boundary region, as reported by Biju et al. [24]. The high frequency semicircular arc results from the relaxation process in the grain interior and the low frequency arc is due to the relaxation in the grain boundary region. It has also been observed that the conduction increases while increasing the temperature. But the relaxation time decreases with increase in temperature. This observation can be attributed to the profound difference between the structures of grain interior and grain boundary regions in nanocrystalline phases. It can be seen that the high frequency arc becomes

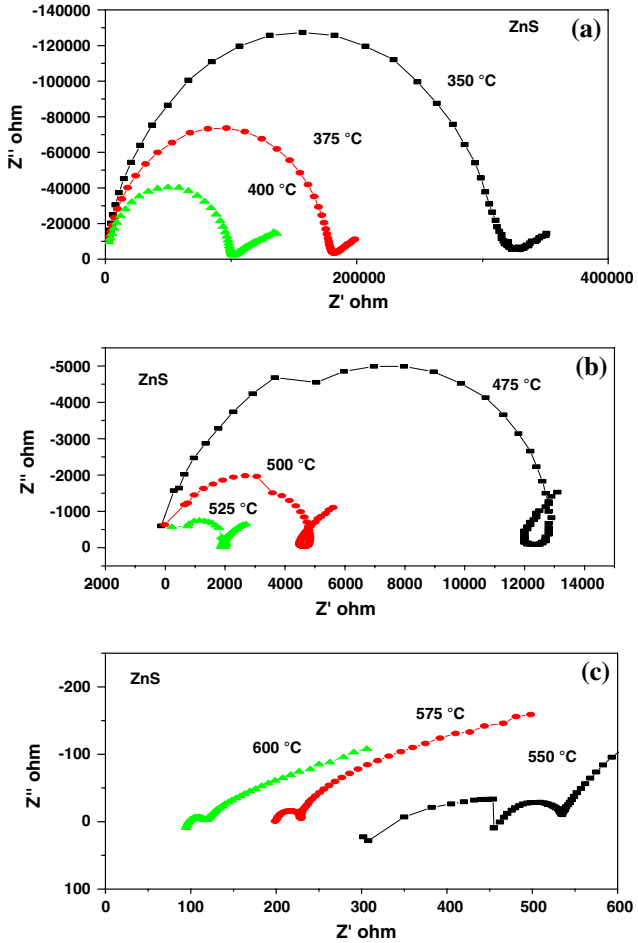

Fig. 5 a–c Impedance spectra at different temperatures for ZnS sample

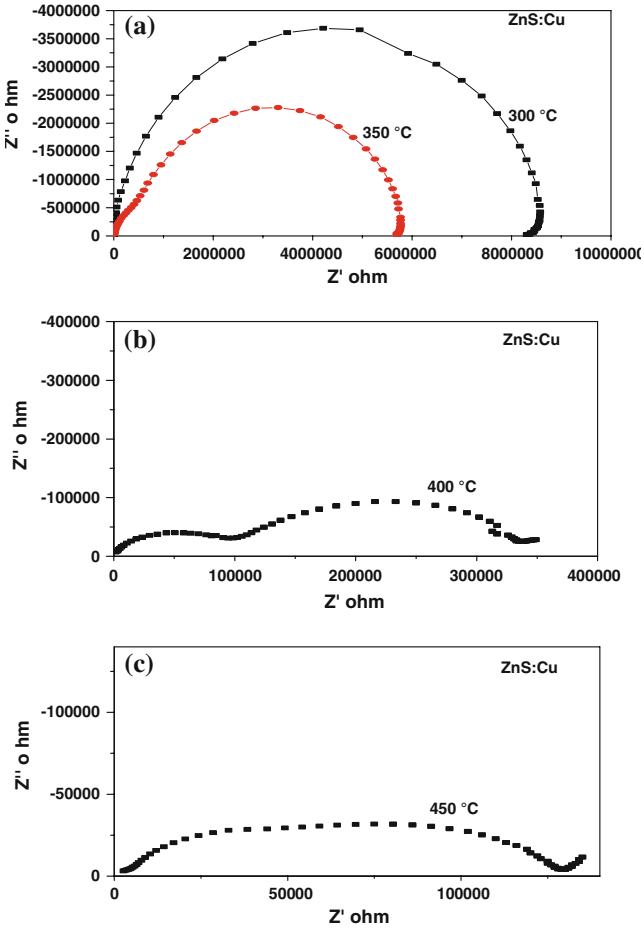

Fig. 6 a–c Impedance spectra at different temperatures for ZnS:Cu sample

larger than the low frequency arc as reported early by Biju et al. [24] and it indicates that the grain boundary disorders decrease thereby enhancing the grain–grain interaction as temperature increases.

At very high temperature region, 500 to 550 °C, the resistance values have decreased from 43677 to 11499 ohm and the corresponding relaxation times are also decreasing from 1.8×10^{-4} to 2.55×10^{-5} s for ZnS:Cu sample. In this region, the conduction increases more and relaxation time again decreases as the temperature increases. Figures 5c and 6c show, for ZnS and ZnS:Cu samples, respectively, that there exists only a single arc and it is attributed to the effect of grain boundary only. This implies that, beyond a particular temperature, there occurs a saturation of the activation of charge carriers.

Figure 7a and b shows the conductivity of both the samples at different temperatures. They reveal the grain contribution mechanism. At very high temperature region, the conduction may be attributed to that across the grain boundaries, and the low temperature conduction may be attributed to the conduction within the grains. Figure 7a and b illustrates the increase in the activation energy with respect to temperature, thereby reflecting the blocking nature of the grain boundaries and also shows the increase in activation energy at very high temperature (nearly 400 °C).

The activation energies as calculated from Fig. 7a and b are 1.71 and 3.64 eV for ZnS and 1.19 and 1.32 eV for ZnS:Cu nanocrystallites and are presented in Table 3. The activation energy is increasing at very high temperature owing to the larger grain interface. The increase in the conductivity with the increase in temperature implies the decrease in defect density [20]. The prepared nanoparticles may contain open volume defects including vacancies. On heating, considerable decrease in the concentration of these defects can be expected which in turn might give rise to an enhancement in the crystalline or more ordered phase of the sample. Figure 7a and b shows the above mentioned phase transition by the change in the slope in the Arrhenius plot for the temperature ~400 °C.

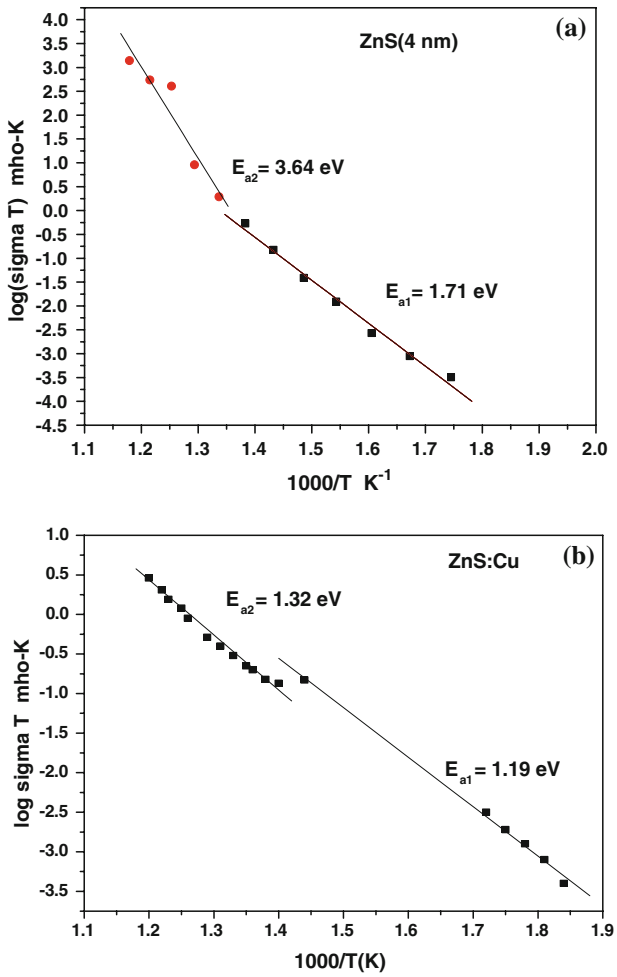

Fig. 7 Arrhenius plot for **a** ZnS and **b** ZnS:Cu samples

Table 3 Activation energies for prepared ZnS and ZnS:Cu samples

Sample	Size (nm)	Activation energies (eV)	
		Defect phase (low temperature region)	Ordered phase (very high temperature region)
ZnS	4	1.71	3.64
ZnS:Cu	3	1.19	1.32

Conclusion

In the present work, ZnS and Cu-doped ZnS nanocrystallites were prepared by chemical precipitation method with average crystallite sizes of 4 and 3 nm, respectively. The XRD and HRTEM measurements confirmed the hexagonal structure of the samples. The effect of electrical conduction through grain interior and grain boundary regions at different temperatures were studied using impedance spectroscopy method. The presence of two distinct relaxation processes associated with the grain interior and grain boundary regions of the nanocrystallites are identified. We concluded that the conduction through the grain boundary regions exceeds the conduction across the regions of intergranular contact. At high temperature, impedance arcs describe that the conduction of grain boundary region is very much greater than that of the grain interior region. At very high temperature, the activation energy increases considerably and is attributed to larger grain interface and therefore, a lower barrier height for the electron to flow. The phase transition indicated by the Arrhenius plots may be attributed to the transition from a defective phase to a more crystalline phase. Hence we get consistent values of activation energy for even very high temperature range.

References

1. Chen S, Liu W (1999) Langmuir 15:8100
2. Nanda J, Sapra S, Sarma DD (2000) Chem Mater 12:1018
3. Chestnoy N, Hull R, Brus LE (1986) J Chem Phys 85:2237
4. Norris DJ, Yao N, Charnock FT, Kennedy TA (2001) Nano Lett 1:3
5. Chen W, Malm JO, Zwiller V, Huang Y, Liu S, Wailenberg R, Bovin JO, Samuelson L (2000) Phys Rev B 61:11021
6. Soo YL, Ming ZH, Huang SW, Kao YH, Bhargava RN, Gallugher D (1994) Phys Rev B 50:7602
7. Awschalom DD, Kikkawa JM (1999) Phys Today 52:33
8. Geng BY, Zhang LD, Wang GZ, Xie T, Zhang YG, Meng GW (2004) Appl Phys Lett 84:2157
9. Bhattacharjee B, Ganguli D, Iakoubovesku K, Stesmans A, Chaudhuri S (2002) Bull Mater Sci 25:175
10. Nanda J, Kuruvilla BA, Sarma DD (1999) Phys Rev B 59:7473
11. Fisher AG (1963) J Electrochem Soc 110:733
12. Mu J et al (2005) Mater Res Bull 40:2198
13. Lee S, Song D et al (2004) Mater Lett 58:342
14. Huang J, Yang Yi, Xue Shanhua et al (1997) Appl Phys Lett 70:2335
15. Fuler ML (1929) Philos Mag 8:658 (version 2.3V)
16. Mazher J, Shrivastav AK, Nandedkar RV, Pandey RK (2004) Nanotechnology 15:572
17. Cullity BD (1978) Elements of X-ray diffraction, 2nd edn. Addison-Wesley, Reading, MA
18. Wang M, Sun L, Fu X, Liao C, Yan C (2000) Solid State Commun 115:493
19. Borchert H, Shevchenko EV, Robert A, Mekis I, Kornowski A, Grubel G, Weller H (2005) Langmuir 21:1931
20. Macdonald Ross (ed) (1987) Impedance spectroscopy, emphasizing solid materials and systems. Wiley, New York
21. Cole KS, Cole RH (1941) J Chem Phys 9:341
22. Almond DP, West AR (1983) Solid State Commun 9–10:277
23. Sinclair DC, West AR (1989) J Appl Phys 66:3850
24. Biju V, Abdul Khadar M (2001) Mater Sci Eng A 304–306:814